REGION
The Journal of ERSA
Powered by WU

Volume 13, Number 1, 2026, 61–94
DOI: 10.18335/region.v13i1.613

journal homepage: region.ersa.org
ISSN: 2409-5370

The General Urban Distortion Propagation Law – A Novel Dynamic Mathematical Framework for Modeling Shock Propagation and Recovery in Complex Urban Systems

Thaer Ayasreh[1]

[1] Independent Researcher, Jerash, Jordan

Received: 25 June 2025/Accepted: 9 March 2026

Abstract. Contemporary cities are increasingly exposed to cascading shocks that propagate through complex and interconnected urban networks, challenging the explanatory power of traditional risk models. This study introduces the General Urban Distortion Propagation Law (GUDPL), an innovative dynamic mathematical framework that integrates functional connectivity, effective distance, time delays, structural vulnerability, recovery dynamics, and irreducible residual effects. The model provides a unified representation of how urban shocks emerge, spread, and attenuate across interconnected systems, and can, in principle, support the identification of vulnerable urban nodes and resilience-oriented planning. To illustrate the operational behavior of the proposed framework, a proof-of-concept simulation based on a stylized cascading power outage scenario is conducted, highlighting delayed propagation, heterogeneous impacts, and recovery processes. GUDPL is adaptable to different crisis types and compatible with time-dependent and real-time modeling contexts, offering a flexible analytical foundation for urban resilience, sustainability, and crisis management research.

Key words: Urban shock propagation, Spatio-temporal modeling, General Urban Distortion Propagation Law (GUDPL), Intercity functional coupling, Cascading failures, Urban recovery models, Urban system resilience

1 Introduction

The twenty-first century is witnessing an unprecedented urban transformation, with cities becoming dominant centers of human activity and economic growth. However, this increasing concentration of population and resources has made urban areas more vulnerable to a variety of shocks. In recent decades, the challenges facing cities have been exacerbated by recurring crises such as natural disasters, pandemics, economic crises, and infrastructure failures. With cities becoming increasingly interconnected through complex networks of relationships, the effects of these shocks are no longer confined to their locations; they now spread across the network to distant cities, causing cascading failures that can lead to widespread paralysis in urban functions (Tang et al. 2025).

This increasing interconnectedness poses a new challenge in understanding the behavior and transmission of urban shocks, necessitating the development of models capable

of representing the spatial and temporal dimensions of shocks to understand complex propagation patterns.

Over the past decades, contemporary literature has produced numerous models that have contributed to our understanding of urban interconnectedness. Gravity models have provided insights into patterns of interaction between cities (Fotheringham, O'Kelly 1989), while complex network theory has elucidated the structural characteristics of urban systems (Batty 2013). Simultaneously, research on resilience has enhanced our understanding of how urban systems respond to and recover from shocks (Meerow et al. 2016). The resilience of urban networks is not only related to physical endurance but is influenced by the level of functional connectivity and the ability to adapt to changes over time (Rahimi et al. 2025). Studies have shown that analyzing the resilience of complex urban networks requires integrating economic, structural, and social links into a multidimensional model (Zhang et al. 2022).

Despite significant progress in modeling urban relationships, most existing models do not capture the complex nature of urban relationships along with the temporal dynamics of shock propagation and lack the integration of recovery mechanisms. They often focus on specific aspects of urban interactions without capturing the multidimensional nature of urban connections. Moreover, most models are static or focus on steady-state conditions, failing to account for the dynamic processes of shock propagation and recovery.

In this context, this study aims to bridge this methodological gap by proposing the General Urban Distortion Propagation Law (GUDPL). GUDPL represents a new, flexible, and dynamic mathematical framework that simulates the transmission of urban distortion across interconnected cities. This model is based on the fundamental hypothesis that the impact of one city's collapse on another depends on the degree of spatial and functional connectivity between them, the magnitude of the gap in urban resilience, and the time required for the shock effect to be transmitted. The model is characterized by its flexibility in adapting to various crises and explaining and predicting the transmission of shocks and recovery across urban networks. It also incorporates essential elements such as structural vulnerability, cascading effects, time delays, and recovery functions, making it a potentially useful analytical framework for understanding urban risks and enhancing preventive planning.

This research includes a presentation of the theoretical foundations upon which GUDPL is based, an explanation of its development methodology, and a presentation of the mathematical formulation of the law and its main components. The research also discusses the potential theoretical and practical significance of the law, identifies current limitations, and suggests directions for future research.

1.1 Theoretical Foundations of Shock and Distortion Propagation in Urban Systems

The General Urban Distortion Propagation Law (GUDPL) is based on a multidisciplinary theoretical framework derived from developments in understanding urban networks, complex systems theory, gravity models, spatial interaction, and urban resilience research. This section aims to review the main theoretical foundations that form the conceptual basis of the law, with reference to relevant previous studies that paved the way for such an integrative model.

1.1.1 Urban Networks: From Hierarchical Structures to Complex Interconnected Systems

Urban network studies have evolved from classical hierarchical models—such as those by Christaller and Lösch, which emphasized the spatial distribution of urban functions—toward more dynamic frameworks focusing on inter-city interactions. The quantitative revolution, led by scholars like Berry (1964) and Pred (1977), expanded urban systems theory, while Wilson (1970) introduced entropy-maximization models that laid a more rigorous mathematical foundation. However, these approaches struggled to capture nonlinear dynamics.

Later, Batty (2005) conceptualized cities as complex adaptive systems, and Bettencourt et al. (2010) demonstrated how urban characteristics scale predictably with size.

In the last decade, big data enabled new empirical insights—Boeing (2021) analyzed global street networks, and Wang et al. (2023) mapped real-world urban interactions using mobile phone data—though such approaches still require integration into explanatory models.

Complex network theory now provides a key framework. The way connections are distributed between cities affects how shocks spread (Barabasi, Pósfai 2016). Concepts like centrality (Borgatti, Brass 2019), cascading failures (Valdez et al. 2020), and percolation thresholds (Dorogovtsev et al. 2008) help explain urban shock propagation. GUDPL builds on this by emphasizing functional coupling (Φ_{ij}) and network topology (Crucitti et al. 2006) to trace pathways of disruption and identify critical urban nodes.

1.1.2 Urban Systems Theory

Urban systems theory views cities as interconnected units engaged in flows of economy, population, services, and information—rather than isolated places. It emphasizes hierarchy (Batty 2005), specialization (Scott, Storper 2015), boundaries (Avni et al. 2022), and emergent properties (Allen 1997). Dynamic models support this theory by simulating how urban variables evolve, aiding GUDPL in analyzing the progression or containment of distortions.

Complex systems theory explains how minor shocks can trigger large-scale failures through cascading effects (Buldyrev et al. 2010). GUDPL integrates this by modeling collapse intensity (E_j), delay (τ_{ij}), and residual distortion ($E_{\min,j}$) to reflect nonlinear spread. Diffusion theory, rooted in geography and sociology (Hägerstrand 1967), also informs this framework. Though typically applied to economics (Zenou et al. 2018), innovation (Arieli et al. 2020), or epidemics (Alrasheed et al. 2024), its principles—like proximity and adoption thresholds—help explain urban shock transmission. GUDPL advances these models by incorporating recovery and structural vulnerability within the urban setting.

1.1.3 Gravitational Models and Urban Shock Transmission

Gravity models have long explained spatial flows by relating interaction strength to city "mass" (e.g., population, GDP) and inversely to distance (Wilson 1970, Fotheringham, O'Kelly 1989). Early contributions by Reilly (1931), Huff (1963), and Wilson (1970) introduced entropy-based refinements. Recent advances, supported by computing and data availability, include multidimensional distances (Tubadji, Rudkin 2025), mobile-data validation (Lenormand et al. 2016), and network effects (Wang et al. 2019).

Yet, these models remain limited in modeling urban shock propagation. They often assume symmetric, static interactions, which contradict the asymmetric and nonlinear nature of crises (Haynes, Fotheringham 1984, Hsu et al. 2021, Yuan et al. 2025). The lack of a temporal dimension further restricts their explanatory power (Fan et al. 2020).

Efforts to address these issues include the radiation model (Simini et al. 2012, Masucci et al. 2013), which removes symmetry and calibration constraints, and dynamic extensions (Yang et al. 2014). However, these remain partial solutions.

GUDPL builds on core gravity concepts—distance decay, attraction, and constraints (Taylor 2022)—but advances them through *effective distance* (d_{ij}), multidimensional decay (k), and integrated temporal-recovery functions, offering a more adaptive, crisis-sensitive framework.

1.1.4 Urban Resilience: From Resistance to Adaptive Transformation

Urban resilience research has evolved to address how cities resist, absorb, and recover from shocks. Definitions and frameworks now emphasize its multidimensional nature—physical, social, economic, and institutional (Meerow et al. 2016, Sharifi, Yamagata 2017). Empirical studies explored responses to terrorism (Coaffee, Lee 2016) and climate disasters (Lv et al. 2024), while quantitative tools such as composite indicators (Cutter et al. 2010), network metrics (Linkov et al. 2022), and integrated models (Markolf et al. 2018, Peiris 2024) have aimed to assess resilience at various scales.

Despite progress, most models lack a dynamic, network-based framework to simulate shock transmission and recovery over time. GUDPL addresses this by integrating key resilience parameters: recovery function $R_j(t-\tau_{ij})$, rate λ_j, and residual impact $E_{\min,j}$. It also incorporates structural vulnerability V_j in calculating collapse intensity E_j, reflecting each city's sensitivity to shocks based on social, environmental, and institutional factors—bridging the gap between resilience assessment and real-time urban shock modeling.

Despite extensive literature, most models remain limited—narrow in focus, static in nature, and lacking in realism or adaptability. They often fail to capture temporal dynamics, cascading effects, or urban variability. GUDPL addresses these gaps by offering a multidimensional, dynamic, and interactive framework that integrates various forms of interconnectedness, models nonlinear propagation and recovery, and adapts to diverse urban contexts. It thus contributes a robust and flexible tool for understanding shock transmission in complex urban systems.

2 Research Materials and Methods

The General Urban Distortion Propagation Law (GUDPL) was developed as a mathematical framework to model how shocks spread across interlinked urban systems. The methodology followed five main stages:

Identifying the Gap : Existing models lacked multidimensional connectivity, temporal dynamics, and asymmetry in representing urban shocks—prompting the need for a more comprehensive framework.

Conceptual Foundation : Core ideas such as functional coupling, effective distance, collapse intensity, recovery rate, and time delay were drawn from urban network theory, spatial interaction, complexity, and resilience literature.

Mathematical Translation : Key variables were formalized—for example, D_i for distortion, E_j for collapse intensity, Φ_{ij} for coupling strength, and $R_j(t-\tau_{ij})$ for recovery. Each component was designed to be flexible, allowing various functional forms based on context and data.

Equation Assembly : Components were integrated into a central equation modeling how distortion in each city evolves over time under intercity influences.

Assumptions and Limitations : Assumptions (e.g., measurability, data availability) and potential challenges (e.g., calibration, empirical validation) were clearly acknowledged.

GUDPL thus merges theoretical rigor with practical flexibility, offering a customizable foundation for analyzing diverse urban shock scenarios and advancing future research.

2.1 General Urban Distortion Propagation Law (GUDPL): Mathematical Model Formulation and Component Interpretation

2.1.1 Core Concept and Scope

The General Urban Distortion Propagation Law (GUDPL) aims to provide a dynamic mathematical framework for estimating the degree of distortion (D_i) in a specific city (i) at a given time (t), resulting from the effects of collapse or shock (E_j) originating from other cities (j) within an interconnected urban network. The law takes into account the strength of functional coupling between cities, effective distance, time delay, cities' recovery capacity, and underlying structural vulnerability.

2.1.2 Fundamental Assumptions

The model is built on three fundamental assumptions:

1. Cities are not independent entities but are interconnected through multiple functional relationships.

2. The impact of shocks decreases with increasing functional distance between cities.

3. Shock propagation follows patterns similar to physical attenuation laws, with non-linear dampening across distance.

2.1.3 Structural Flexibility

One of the main strengths of the law is its structural flexibility and adaptability to various types of urban crises. The model does not rely on predetermined fixed parameters but has been designed according to a flexible modeling structure that allows customization of its components based on the nature of the shock. Whether the crisis is caused by earthquakes, climate disasters, pandemics, infrastructure failures, or economic collapse, the internal variables of the model can be recalibrated based on specific indicators and scenarios.

2.1.4 Basic Equation of the GUDPL Model

Based on the previous assumptions, the static model of GUDPL has been formulated as follows:

$$D_i = \sum_{j=1}^{n} \left(\frac{E_j \Phi_{ij}}{d_{ij}^k} \right) + \varepsilon_i \tag{1}$$

2.1.5 Temporal model

In light of the limitations of the static model, a temporal model was constructed that takes into account the evolution of collapse intensity over time. The mathematical formulation of the dynamic temporal model is as follows:

$$D_i(t) = \sum_{j=1}^{n} \left(\frac{E_j(t) \Phi_{ij}(t)}{[d_{ij}(t)]^{k(t)}} \right) + \varepsilon_i(t) \tag{2}$$

where:

$D_i(t)$: The total degree of urban distortion in the city (i) at time t.

$E_j(t)$: The time-varying collapse intensity or shock severity in source city j at time t. It reflects the evolving magnitude of disruption in the source city and may be estimated through normalized indicators related to infrastructure failure, economic decline, service disruption, health-system stress, or other crisis-specific dimensions.

$\Phi_{ij}(t)$: The functional coupling factor between the city i and j at time t.

$d_{ij}(t)$: The effective distance between the city i and j at time t.

$k(t)$: The distance attenuation factor, a positive exponent that reflects how quickly the shock effect dissipates with increasing effective distance.

$\varepsilon_i(t)$: The random factor or 'chance' or 'external fluctuations in the model at time t'.

The basic components of the model

1. Degree of urban distortion $(D_i\,(t))$:

   A composite indicator reflecting the degree of disruption experienced by city i due to external shocks. Its composition can be adapted to the type of shock being studied.

2. Vulnerability-adjusted collapse severity (E_j)

   A component that can be customized according to the nature of the shock. It is calculated using a weighted average of a set of sub-indicators, as follows:

$$E_j = V_j \sum_{m=1}^{\mathrm{ME}} w_m I_{jm}$$

Here, V_j acts as an amplifier of collapse severity; higher structural vulnerability increases the realized collapse intensity for a given shock magnitude.

Where:

E_j : The severity of the total collapse of the city j. It expresses the extent of the city's collapse in terms of the nature of the crisis, and the closer E_j is to 1, the greater the intensity of the collapse (or the opposite according to the definition).

I_{jm} : The sub-indicator m that is selected and normalized according to the nature of the crisis; for example, collapse indicators suitable for an earthquake or flood (infrastructure + public services + health services), and in the case of a specialized crisis such as a power outage (energy availability + network efficiency), and economic collapse (GDP, unemployment, market activity, supply chains). The indicators I_{jm} are normalized according to the Min-Max Normalization Linear Normalization formula or by converting them to the range [0, 1] to avoid measurement bias.

w_m : The weight of indicator m adjusted according to the importance of each indicator in the context of the crisis; for example, in the case of earthquakes, a higher weight may be given to infrastructure compared to the economy).

M : The number of sub-indicators used in the assessment should preferably be ≥ 3 to cover multiple dimensions (economic, social, and basic functional).

V_j : The structural vulnerability of city j is calculated as a weighted average of m normalized sub-indicators $V_{j\rho}$, reflecting the city's susceptibility to long-term or cascading distortions. These indicators cover domains such as infrastructure (e.g., decay rate), economy (e.g., sectoral dependency), governance (e.g., corruption levels), society (e.g., social cohesion), and health (e.g., sustainable coverage). Each dimension is assigned a weight (α_ρ) based on its relative importance. All indicators are scaled to [0, 1] and aggregated to form V_j, as follows:

$$V_j = \sum_{\rho=1}^{M_V} \alpha_\rho V_{j\rho}$$

3. Functional Coupling Factor (Φ_{ij})

Reflects the structural and functional connectivity between two cities. The basic linear formula:

$$\begin{aligned} \Phi_{ij} &= \omega_1 L_{ij}^{(1)} + \omega_2 L_{ij}^{(2)} + \ldots + \omega_R L_{ij}^{(R)} \\ &= \sum_{r=1}^{R} \omega_r L_{ij}^{(r)} \end{aligned}$$

where:

Φ_{ij} : The total functional coupling index between city i and city j, taking a value in the range [0, 1], where a higher value indicates a stronger functional linkage.

L_{ij}^{r} : The degree of linkage between cities i and j for a given linkage type r is represented as a normalized value between 0 and 1, reflecting the strength of interdependence. Linkage types are selected based on the nature of the crisis, as different shocks influence networks in different ways. For instance, in a national power grid failure, relevant linkages may include megawatts of electricity exchanged (electrical linkage), number of trucks or supply lines (logistical linkage), cross-city use of services such as hospitals (service linkage), proportion of j's industrial electricity sourced from i (economic linkage). This modular structure allows GUDPL to adapt the definition and weight of linkages based on shock-specific dynamics.

ω_r : Each linkage type r is assigned a weight ω_r, representing its relative importance in the context of the specific crisis (Weighted Importance of Linkage Types). These weights are calibrated so that their total across all R types satisfies the condition:

$$\sum_{r=1}^{R} \omega_r = 1, \qquad \omega_r \geq 0$$

This weighting ensures that the composite functional coupling reflects not just the presence of connections, but their contextual relevance to the type of shock being analyzed.

R : The number of linkage dimensions used in constructing the index varies by crisis type. These may include economic, service, health, social, political, security, logistical, or electrical connections, among others—selected based on their relevance to the specific shock scenario.

The extended form (with nonlinear interactions)

To enhance the accuracy of the model, synergistic or competitive effects between types of connectivity can be integrated:

$$\begin{aligned} \Phi_{ij} &= \left(\omega_1 L_{ij}^{(1)} + \ldots + \omega_R L_{ij}^{(R)}\right) + \left(\lambda_{12} L_{ij}^{(1)} L_{ij}^{(2)} + \ldots + \lambda_{(R-1)R} L_{ij}^{(R-1)} L_{ij}^{(R)}\right) \\ &= \sum_{r=1}^{R} \omega_r L_{ij}^{(r)} + \sum_{\substack{r,\, s = 1 \\ r \neq 1}}^{R} \lambda_{rs} L_{ij}^{(r)} L_{ij}^{(s)} \end{aligned}$$

where:

λ_{rs} : The coefficient λ_{rs} captures the interaction between linkage types r and s. A positive value ($\lambda_{rs} > 0$) indicates a reinforcing relationship – where one linkage amplifies the effect of the other – while a negative value ($\lambda_{rs} < 0$) indicates a competitive or inhibitory relationship. For example:

- In pandemics, increased social interaction can intensify health system strain.
- In security crises, political conflict may weaken intercity security coordination.
- In displacement scenarios, mass movement may overwhelm administrative capacities, reducing effective response across the network.

Effective Distance (d_{ij}): Concept and Formula

d_{ij} represents the effective distance between cities i and j, extending beyond mere geographic separation. It quantifies the level of *resistance* or *functional separation* between the two cities and can incorporate spatial, temporal, structural, and behavioral factors depending on the crisis context. For instance, high travel time, poor connectivity, or administrative barriers may increase d_{ij} even if the geographic distance is small. A flexible general formula for effective distance is:

$$d_{ij}^{k} = \left(\sum_{q=1}^{Md} \Phi_q X_{ij}^{q} \right)^{k}$$

where:

$X_{ij}^{(q)}$: Effective distance d_{ij} is constructed from a set of M sub-dimensions, each representing a specific form of separation between cities i and j, normalized to a [0, 1] scale. Relevant dimensions vary by crisis and may include (1) Geographic distance (e.g., kilometers), (2) Temporal distance (e.g., travel time), (3) Institutional distance (e.g., administrative divergence), (4) Structural distance (e.g., infrastructure or resource disparities), (5) Behavioral distance (e.g., social or cultural variation), (6) Economic distance, among others.

Φ_q : represents the relative weight assigned to each distance dimension m, indicating its significance in the model based on the nature of the crisis. The weights are normalized to satisfy the condition:

$$\sum_{q=1}^{Md} \Phi_q = 1, \ \Phi_q \geq 0$$

Md : Number of dimensions of distance. It is determined by the complexity of the model (usually between 3 to 5 dimensions).

In cases where distance dimensions are overlapping, strongly interdependent, or exhibit nonlinear interaction effects, an alternative formulation can be adopted:

$$d_{ij} = \sqrt{\sum_{q=1}^{Md} \Phi_q \left(X_{ij}^{(q)} \right)^2}$$

which captures overlapping or reinforcing distance effects. In the illustrative simulation presented in this study, distance dimensions are treated as independent, and the additive composite formulation is therefore employed.

This formulation corresponds to a weighted Euclidean distance and is included to highlight the structural flexibility of the GUDPL framework rather than to impose a mandatory modeling choice.

4. Attenuation Factor k

This factor determines how quickly the effect of the shock decreases with increasing effective distance:

$k = 1$: The effect decreases linearly with distance

$k > 1$: The effect decreases rapidly with distance (suitable for local crises)

$k < 1$: The effect decreases slowly with distance (suitable for global crises)

5. The Stochastic Error Term ε_i

   The term ε_i captures random fluctuations or unexplained external factors not accounted for by the core components of the model. These may include (1) Sudden political events (e.g., coups, border closures), (2) Additional natural disasters (e.g., local floods), (3) Behavioral anomalies or data distortion (e.g., social panic), (4) Measurement errors or reporting inconsistencies.

   In experimental modeling, ε_i is typically assumed to follow a normal distribution: $\varepsilon_i \sim N(0, \sigma^2)$. In simulation, a fluctuation range (e.g., $\pm 5\%$) or scenario-based assumptions may apply. In regression, it represents the residual error.

2.1.6 Time-Delayed Dynamic Model

While dynamic time models offer a more realistic view of collapse evolution, they often assume instantaneous shock transmission between cities – an oversimplification of real urban dynamics. In reality, transmission times vary based on functional distance, connectivity levels, and the type of shock. To address this, the temporal model integrates a delay factor (τ_{ij}), representing the time it takes for a shock to move from city j to city i. This spatial-temporal integration enhances the accuracy of simulating distortion spread across interconnected urban systems. The time-delayed model is expressed as:

$$D_i(t) = \sum_{j=1}^{n} \left(\frac{E_j(t - \tau_{ij}) * \Phi_{ij}(t - \tau_{ij})}{[d_{ij}(t)]^{k_i(t)}} \right) + \varepsilon_i(t) \tag{3}$$

where:

$E_j(t - \tau_{ij})$: The intensity of the collapse or the effective shock in city j at time $(t - \tau_{ij})$, taking into account the time delay for the impact to reach city i.

τ_{ij} : The time delay between the occurrence or development of the shock in city j and the arrival of its impact to city i. It depends on the nature of the crisis, the type of pathway through which the impact travels, and the effective distance.

τ_{ij} can be calculated based on the type of crisis. The most common, for example, are: in the case of a direct earthquake, $\tau_{ij}(t)$ is estimated based on the time it takes for emergency teams or shock waves to arrive (minutes – hours). In the case of a power outage, it is estimated by the time the electricity is cut off in city i after being cut off from j. In the case of an economic crisis, it is estimated by the time the market i is affected after a crisis in j (days – months). In the case of population displacement, it is estimated by the time city i starts receiving refugees or displaced persons from j (days – weeks). In addition, $\tau_{ij}(t)$ can be calculated based on historical data, if data from previous crises exists, determine the moment of collapse in city j, then moment m of the impact on city i, and then calculate the difference. The $\tau_{ij}(t)$ can also be calculated by dividing the effective distance between the two cities by the speed of wave propagation according to its type (for example: the speed of electrical outages, the speed of disease transmission, etc.).

2.1.7 The complete form of the GUDPL model with the recovery function

In real urban systems, shock impacts unfold over time rather than occurring in a single instant. Their duration and decay depend on system fragility, interconnectivity, and recovery capacity. To capture this, GUDPL incorporates an extended temporal model that simulates how a shock spreads after a time delay (τ_{ij}) and then gradually diminishes in the affected city through a recovery function—exponential, logistic, or linear—guided by a city-specific recovery rate (λ_j).

The model also includes a fixed minimum residual impact ($E_{\min,j}$), reflecting the irreversible structural damage. This formulation allows GUDPL to simulate not only the spread and peak of urban distortion, but also long-term stabilization, deterioration,

Table 1: The Structural Interpretation of $E_{\min,j}$

$E_{\min,j}$	Structural Interpretation
0	The city does not suffer from chronic structural weakness — its complete recovery after the shock is possible
0.2-0.4	Moderate structural weakness: some structures or sectors do not fully recover.
0.5-0.7	Significant or chronic weakness: the city is structurally fragile even in normal conditions.
0.8-1	The city is highly exposed, threatened by continuous collapse even after the shock has ended.

or partial recovery—enabling policy testing and comparative analysis of urban resilience based on varying recovery dynamics, as follows:

$$D_i(t) = \left[\sum_{j=1}^{n} \frac{\left[E_{\min,j} + (E_0(j) - E_{\min,j}) R_j(t - \tau_{ij}(t))\right] \Phi_{ij}(t - \tau_{ij}(t))}{[d_{ij}(t)]^{k_i(t)}} \right] * R_s(t - t_0) + \varepsilon_i(t) \tag{4}$$

where:

$D_i(t)$: The total urban distortion in city i at time t.

$E_0(j)$: The initial collapse intensity in city j.

τ_{ij} : The time delay in shock transmission from j to i.

$\Phi_{ij}(t - \tau_{ij})$: The functional coupling factor at the delayed time.

d_{ij} : The effective or functional distance between the two cities.

$k_i(t)$: The dynamic attenuation coefficient in city i.

$\varepsilon_i(t)$: The error coefficient or random external effects.

$E_{\min,j}$: Represents the irreducible level of distortion in city j, the portion of the shock impact that persists over time, even after recovery. Examples include chronic infrastructure damage or long-term social marginalization. The value ranges between 0 and 1 (see Table 1) and can be estimated through (a) a *composite index* based on structural vulnerability indicators, or *expert judgment*, depending on data availability and context.

$R_j(t - \tau_{ij})$: The standard recovery function for city j after the shock reaches it (post-delay τ_{ij}). It ranges between 1 (at the onset of impact) and 0 (full recovery), modeling how the residual collapse intensity decays over time due to emergency response, external support, and infrastructure restoration. The function reflects the city's dynamic recovery trajectory within the GUDPL framework.

Examples of types of $R_j(t)$ functions:

The recovery function $R_j(t)$ models how collapse intensity in city j decreases over time. Its form depends on the crisis context and data availability. Common types include:

- Exponential function $\longrightarrow R_j(t) = e^{-\lambda_j t}$
- Linear function $\longrightarrow R_j(t) = 1 - \gamma t$
- Logistic function $\longrightarrow R_{j(t)} = \frac{1}{1+ae^{\{-\lambda_j t\}}}$
- Function derived from real data $\longrightarrow R_j(t) = f_{\text{empirical}}(t)$

These formulations allow flexible modeling of diverse urban recovery patterns under different shock scenarios.

λ_j : represents the recovery rate of city j, indicating how quickly the city regains functionality after a shock. Its value depends on factors such as crisis type, institutional capacity, and the city's level of integration within the urban network. A higher λ_j implies faster recovery, while lower values reflect prolonged vulnerability.

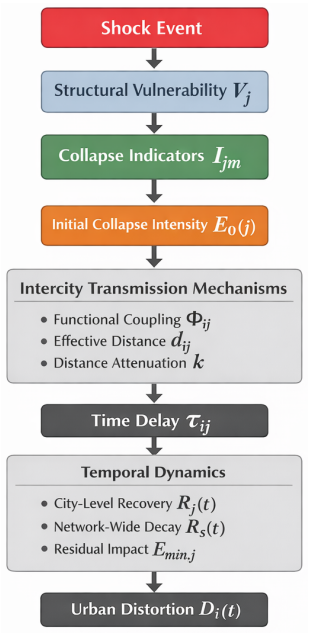

Figure 1: Conceptual flowchart of the General Urban Distortion Propagation Law (GUDPL)

$R_s(t - t_0)$: Represents the overall temporal regression of shock effects across the entire urban network, reflecting how systemic impact fades over time. Like city-level recovery functions, it ranges between 0 and 1 and can follow exponential, logistic, or linear decay. Yet it captures network-wide attenuation, not individual city recovery.
It reflects the "residual shadow" of the shock across the system and can be estimated using *time series* of affected cities, or *aggregated network response* data.

t_0 : The peak moment or the actual beginning of shock propagation in the network, either determines as a constant (for example, the date of the event) or is based on the largest time delay in the network.

Additional considerations and interpretations:

Iterative Computation : $D_i(t)$ is calculated iteratively, where the current distortion in city i depends on past distortions in other cities (including itself), adjusted for time delays. This requires *stepwise temporal simulation*.

Calibration and Validation : Parameter estimation (e.g., Φ_{ij}, V_j, k, τ_{ij}, λ_j, ω_r) is complex and demands *rich data*, advanced modeling techniques, or expert input. Model outputs should be validated against historical shock propagation patterns.

Flexibility : GUDPL allows *adaptive component functions*. Elements like Φ_{ij} or $R_j(t)$ can be tailored – or even made dynamic – to reflect evolving urban conditions or crisis types.

Figure 1 summarizes the sequential modeling stages of the GUDPL framework, from shock definition and city-level structural conditions to intercity transmission mechanisms, temporal dynamics, and the resulting urban distortion. The flowchart is intended to support interpretability of the mathematical formulation and does not replace the formal equations presented in Section 2.

2.2 Parameter Weighting and Calibration Strategy

The GUDPL framework incorporates multiple weighted components, including structural vulnerability weights, collapse severity weights, functional coupling weights, and effective-

distance barrier weights. Given the multidimensional nature of the model, weight calibration is treated as a flexible and context-dependent process rather than a fixed universal specification.

At the model-development stage, the framework explicitly distinguishes between theory-informed, scenario-specific weighting and empirically calibrated weighting. In applied or empirical implementations, several established methodological pathways can be used to estimate or calibrate the weights associated with different GUDPL components, depending on data availability, scale, and research objectives.

First, expert-based multi-criteria decision methods, such as the Analytic Hierarchy Process (AHP), can be used to derive weights for vulnerability dimensions, collapse severity indicators, or distance barriers. AHP is particularly suitable when expert knowledge about causal precedence and relative importance is available, as is often the case in infrastructure resilience and disaster risk management. Pairwise comparison matrices can be constructed for each indicator set, and consistency ratios can be used to ensure internal coherence.

Second, data-driven statistical approaches can be employed when sufficient quantitative observations are available. Entropy-based weighting methods allow weights to be inferred from the variability and informational contribution of each indicator, assigning higher weights to dimensions with greater discriminatory power across cities. Similarly, principal component analysis (PCA) or related factor-analytic techniques can be used to reduce dimensionality and derive implicit weights based on explained variance, particularly for vulnerability or coupling indicators that exhibit strong correlations.

Third, in contexts where time-series or large-scale network data are available, machine learning–assisted calibration can be applied. Supervised learning models (e.g., regularized regression, gradient boosting) may be used to estimate weights by minimizing prediction error against observed impact or recovery trajectories from historical shock events. Regularization techniques (e.g., LASSO or ridge penalties) can mitigate multicollinearity and improve parameter identifiability. Unsupervised learning approaches can also support clustering and feature extraction prior to weight assignment.

Importantly, empirical calibration is not required to estimate all parameters simultaneously. In practice, a staged calibration strategy can be adopted, whereby vulnerability weights, coupling weights, distance barriers, and recovery parameters are estimated sequentially using distinct data sources. This staged approach reduces identifiability problems and aligns with best practices in complex systems modeling.

Overall, the GUDPL framework is designed to accommodate multiple calibration strategies while maintaining internal consistency. The choice of weighting method should be guided by the shock type, spatial scale, data availability, and analytical purpose, allowing the model to balance generalizability with contextual specificity.

2.3 Parameter Identifiability and Dependence Considerations

Given the multi-component structure of the GUDPL framework, not all parameters are intended to be estimated simultaneously in empirical applications. The model explicitly acknowledges potential identifiability challenges and high correlation among parameters, particularly between functional coupling Φ_{ij}, effective distance d_{ij}, vulnerability V_j, and recovery rates λ_j. Estimating all parameters jointly from a single dataset may lead to multicollinearity and unstable parameter estimates.

To address this issue, GUDPL is designed to support a staged and modular calibration strategy, whereby parameters are estimated sequentially or conditionally rather than simultaneously. Structural vulnerability parameters (V_j) and collapse severity components (E_j) can be calibrated independently using static or cross-sectional data prior to dynamic simulation. Functional coupling (Φ_{ij}) and effective distance components (d_{ij}) can then be inferred using network-based or flow data, while recovery parameters (λ_j) are estimated separately from post-shock time-series observations.

This staged approach reduces parameter interdependence and improves identifiability by leveraging distinct data sources and temporal windows for different parameter groups. Where residual correlation persists, regularization techniques (e.g., ridge or

LASSO penalties) or dimensionality-reduction methods (e.g., principal component analysis) can be applied to stabilize estimation without altering the structural form of the model.

Importantly, the proof-of-concept simulation presented in this study does not rely on empirical parameter estimation and therefore does not suffer from identifiability constraints. Instead, it serves to demonstrate the internal logic and dynamic behavior of the model under controlled, theory-consistent parameter settings. Full empirical identification and sensitivity analysis are explicitly deferred to future applied studies.

3 Research Results

The General Urban Distortion Propagation Law (GUDPL) offers an integrated mathematical framework for understanding how urban shocks propagate through complex, interconnected city networks. The results reported here derive from analytical inspection of the model structure and from a transparent proof-of-concept simulation designed to illustrate dynamic behavior under stylized conditions. These results demonstrate the model's capacity to overcome the limitations of classical, one-dimensional approaches by incorporating three essential dimensions:

1. Spatial dimension, represented by effective intercity distance.
2. Functional dimension, captured by intercity coupling across economic, social, and service layers (Φ_{ij}).
3. Temporal dimension, introduced through time-delay effects (τ_{ij}) and variable recovery functions (λ_j).

Furthermore, the model incorporates city-specific structural fragility V_j, which modulates the overall shock intensity based on latent vulnerabilities such as poor infrastructure, economic monocultures, or weak institutional capacities. This factor plays a decisive role in explaining why certain cities experience amplified distortions despite being geographically distant or less connected functionally.

The output D_i is a unit-less composite index that quantifies the cumulative distortion experienced by city i, resulting from shocks propagated across all functionally or spatially connected nodes. It is computed as a weighted aggregation of source intensities E_j, modulated by functional coupling Φ_{ij}, effective distance d_{ij}, and temporal dynamics – including propagation delays τ_{ij} and recovery rates λ_j – along with a stochastic term ε_i. Because its components span different scales and units, the analytical formulation of $D_i(t)$ may include stochastic disturbances. In empirical implementations, however, $D_i(t)$ can be reported as a nonnegative operational index (e.g., by truncation at zero or through min–max normalization). This reporting choice is applied solely at the presentation stage and ensures interpretability, comparability across cases, and consistency with the conceptual meaning of urban distortion. In practical interpretation, values of $D_i \approx 0$ indicate negligible or no impact, values around 1 typically reflect significant functional or structural disturbance, while values exceeding 2 (depending on empirical calibration) suggest the onset of cascading failure—particularly in structurally fragile or centrally positioned cities.

The illustrative simulation reveals that shock propagation is neither homogeneous nor linear. Instead, it follows complex trajectories shaped by the strength of functional ties, localized structural vulnerabilities, and temporal lags. Cities with high centrality within the network often emerge as critical nodes—acting either as conduits or buffers—depending on their resilience capacity.

The simulation illustrates the existence of regime-like transitions, where marginal increases in local shock intensity produce disproportionately larger systemic effects – suggesting the presence of critical thresholds, where small local shocks can escalate into widespread systemic disturbances via non-linear amplification mechanisms. This behavior aligns with principles from complexity theory and highlights the importance of early warning indicators.

Another key innovation lies in the dual-level recovery structure:

- Local recovery $R_j(t)$ based on city-specific characteristics.
- Network-wide recovery $R_s(t)$, which reflects the broader system's return to stability.

Importantly, GUDPL recognizes the existence of residual distortion ($E_{\min,j}$), indicating that some structural damage may persist even after recovery. This insight challenges the notion of full reversibility and underscores the need for adaptive planning strategies.

Finally, the model's modular architecture enables calibration and customization based on the nature of the crisis. Parameters such as ω_r, Φ, k, and λ_{rs}) can be adjusted using historical data or machine learning, allowing for broad applicability across different urban disruption scenarios.

3.1 Proof-of-Concept Simulation: Cascading Power Outage Scenario

To illustrate the dynamic behavior of the General Urban Distortion Propagation Law (GUDPL), a proof-of-concept simulation is conducted using a stylized cascading power outage scenario. This simulation is designed to demonstrate how urban distortion propagates through an interconnected urban network when transmission delays, functional coupling, distance-based attenuation, and recovery dynamics are jointly considered.

In this proof-of-concept, all model weights are intentionally specified using a theory-informed, scenario-specific approach. The purpose is not empirical estimation or predictive validation, but to demonstrate the internal coherence, dynamic behavior, and operational feasibility of the GUDPL framework under a stylized yet plausible shock scenario. Accordingly, the selected weights reflect established causal hierarchies documented in the urban resilience and cascading failure literature and are treated as illustrative rather than empirically optimized parameters. Future empirical applications may recalibrate these weights using the methods outlined in Section 2, without requiring structural modification of the underlying equations. This proof-of-concept should therefore be interpreted as a behavioral demonstration of the model, not as an empirical test of parameter values.

The simulated network consists of five cities (A–E) connected through directed functional linkages reflecting electricity exchange capacity, industrial dependence, and operational interconnection. City A serves as the primary shock origin, representing a major power system failure that initiates a cascading blackout. The simulation is conducted over a discrete time horizon of eight time steps, interpreted as hourly intervals.

Urban distortion is computed using the time-delayed GUDPL formulation with recovery, as defined in Section 2. Transmission delays explicitly govern the timing of shock arrival across cities, while distance-based attenuation and functional coupling regulate the magnitude of propagated impacts. City-level recovery processes gradually reduce collapse intensity over time, and a network-wide attenuation term captures system-level stabilization effects. For clarity of interpretation, stochastic disturbances are excluded in this illustrative run.

The illustrative outcomes of the simulation are presented in Figure 2. The distortion trajectories visually illustrate the characteristic behaviors captured by the GUDPL framework across the affected cities. Distortion emerges only after $t = 2$, reflecting the role of transmission delays. City B, characterized by strong functional coupling and low effective distance to the shock source, experiences a rapid and pronounced distortion peak. In contrast, Cities D and E exhibit cumulative and temporally staggered responses, reaching their peaks at $t = 3$ after aggregating impacts from multiple upstream sources. Over time, distortion levels decline as recovery unfolds, yet remain strictly positive due to the presence of irreducible residual effects ($E_{\min,j}$), capturing the long-tail persistence of structural impacts following the crisis.

The complete numerical operationalization of all model components, including parameter values, weighting rationales, and step-by-step calculations, is provided in the Appendix to ensure transparency and replicability.

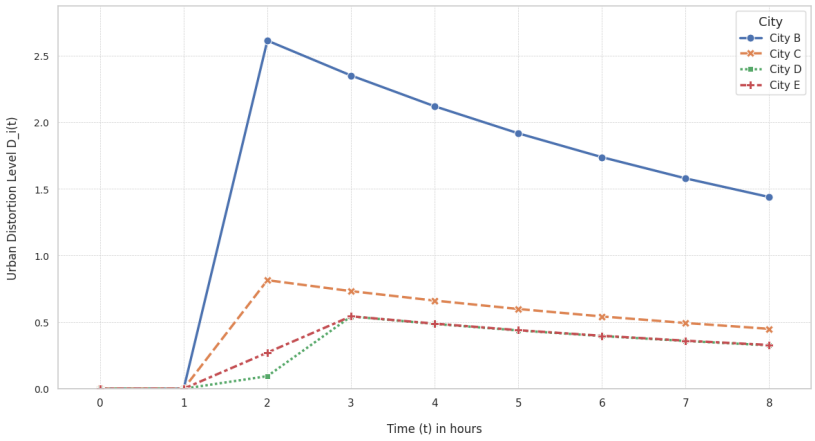

Figure 2: Urban Distortion Trajectories $D_i(t)$ for Affected Cities Following a Cascading Blackout

4 Discussion

The General Urban Distortion Propagation Law (GUDPL) represents an attempt to develop an integrated mathematical framework for understanding the dynamics of shock propagation in complex urban systems. This approach transcends the fundamental limitations of traditional gravity models identified by Haynes, Fotheringham (1984) and Hsu et al. (2021), which assume symmetrical and static interactions between cities. Instead, GUDPL provides a dynamic framework that allows for the representation of asymmetrical and time-varying interactions, aligning with recent trends in spatial interaction modeling.

The model also surpasses the limitations of radiation models developed by Simini et al. (2012) by introducing the concept of "functional coupling" (Φ_{ij}), which goes beyond the notion of a city's fixed "mass" to encompass multidimensional dynamic links. This development addresses the criticism raised by Fan et al. (2020) regarding the absence of a temporal dimension in traditional models, providing a more realistic representation of how urban systems evolve over time in response to disturbances.

GUDPL explicitly incorporates urban resilience concepts developed by Meerow et al. (2016) and Sharifi, Yamagata (2017). While previous studies focused on assessing resilience as a static property of individual cities, GUDPL offers a dynamic understanding of resilience as a process that evolves over time and is influenced by inter-city connectivity. This aligns with the trend identified by Rahimi et al. (2025) regarding the importance of understanding resilience in the context of functional connectivity between urban centers.

The "recovery function" ($R_j(t-\tau_{ij})$) in the model goes beyond simplistic approaches to linear recovery, reflecting the complex nature of urban recovery processes documented in case studies such as Coaffee, Lee (2016) and Lv et al. (2024). Similarly, the concept of "minimum residual distortion" ($E_{\min,j}$) reflects the reality noted in the literature about the impossibility of complete return to the original state after major shocks, acknowledging the permanent transformations that often follow significant disruptions.

GUDPL expands the applications of complex network theory in studying urban systems, moving beyond the static structural analyses presented by Batty (2013) and Bettencourt et al. (2010). By incorporating temporal dynamics and cascading effects, the model provides a framework for understanding how urban networks evolve in response to shocks, addressing an aspect insufficiently covered by previous models. The cascading failure mechanism in the model aligns with the theoretical work of Valdez et al. (2020) and Buldyrev et al. (2010), but adds a specific spatial and temporal dimension that reflects the uniqueness of urban systems.

Despite its theoretical strength, the practical application of the model faces significant challenges related to measuring its key variables. For instance, measuring "functional coupling" (Φ_{ij}) requires comprehensive data on economic, social, and informational flows

between cities, which may not be readily available, especially in developing countries (Cutter et al. 2010).

Potential empirical operationalization of the GUDPL framework can draw on established international data sources. Urban structural and socioeconomic indicators relevant to vulnerability and recovery can be obtained from UN-Habitat, the World Bank (e.g., World Development Indicators), and national statistical offices. Data on infrastructure performance, energy systems, and service disruptions may be sourced from sectoral agencies and utility operators, while intercity flows and functional linkages can be approximated using transportation statistics, trade data, or mobility datasets. These sources provide a feasible empirical foundation for future calibration and validation efforts.

The GUDPL framework is inherently compatible with recent advances in computational modeling and network science. Its formulation allows direct integration with network metrics such as centrality, betweenness, and modularity to identify systemically important cities and critical transmission pathways. Functional coupling parameters (Φ_{ij}) can be informed by network-based measures derived from mobility, infrastructure, or economic flow data, while effective distance metrics can be refined using weighted or multilayer network representations. Moreover, artificial intelligence and machine learning techniques offer promising avenues for operationalizing GUDPL in applied contexts. Data-driven models can support parameter calibration, early-warning detection, and scenario exploration without altering the underlying mathematical structure of the law. Importantly, such techniques are viewed as complementary tools for estimation and monitoring rather than substitutes for the analytical core of the model. This compatibility positions GUDPL as a flexible bridge between theory-driven urban systems modeling and emerging computational approaches.

Determining accurate values for model parameters, such as the "distance decay coefficient" (k) and "recovery rate" (λ_j), requires intensive empirical studies. This aligns with observations by Markolf et al. (2018) regarding methodological challenges in modeling infrastructure resilience. The model also faces challenges in empirical verification and calibration due to the scarcity of comprehensive data on urban shock propagation, a challenge that aligns with observations by Yang et al. (2014) on the difficulties of modeling the temporal dynamics of crises.

GUDPL can be compared with other integrated frameworks proposed by researchers such as Peiris (2024) and Linkov et al. (2022). While these frameworks focus on specific aspects of resilience (such as infrastructure resilience or flood resilience), GUDPL provides a more general framework that can be applied to multiple types of shocks. However, this generality may come at the expense of precision in specific contexts, highlighting the trade-off between generalizability and contextual specificity in resilience modeling.

The application of the model could be enhanced through the utilization of big data techniques referenced by Boeing (2021) and Wang et al. (2023). For example, social media data and mobile phone data could be used to estimate functional coupling between cities, while satellite data could be used to track physical changes associated with shocks. These data sources offer new opportunities for operationalizing the model's theoretical constructs in real-world settings.

The model could be translated into practical decision support tools, similar to what Sharifi, Yamagata (2017) proposed. These tools could help planners and policymakers assess systemic risks and design resilience strategies that account for the interconnected nature of urban systems. The scope of the model's application could also be expanded to include different levels of spatial analysis, aligning with recent trends in studying multi-level urban systems, as in the work of Scott, Storper (2015).

5 Conclusion

The General Urban Distortion Propagation Law (GUDPL) represents a significant step toward a deeper understanding of shock propagation dynamics in complex urban systems. By developing a mathematical framework that integrates spatial, temporal, and functional dimensions of urban connectivity, this research makes an original contribution to the fields of urban planning, risk management, and resilience studies.

The findings of this research confirm that cities are not isolated entities but nodes in a functionally interconnected network, where shocks travel and amplify through multidimensional links. This understanding transcends traditional models that have focused on the individual resilience of cities, emphasizing instead the importance of understanding resilience as a property of the urban system as a whole. The interconnected nature of urban systems means that disturbances rarely remain localized but propagate through established functional connections, creating complex patterns of impact that cannot be predicted through simple linear models.

This research highlights the importance of the temporal dimension in understanding urban shock dynamics. Time delays in effect transmission, varying recovery rates between cities, and the evolving nature of functional links all contribute to shaping the temporal trajectory of distortion propagation and containment. This temporal dimension is essential for developing proactive strategies to mitigate risks and enhance resilience, moving beyond reactive approaches that often characterize traditional urban planning.

The study emphasizes the importance of recognizing variations in structural vulnerability and recovery capacity among different cities. Cities differ in their economic structures, infrastructure, and social institutions, and consequently in their ability to absorb shocks and recover from them. This variation must be taken into account when designing resilience policies and allocating resources, suggesting a need for context-specific rather than one-size-fits-all approaches to urban resilience.

The illustrative results indicate that shock propagation in urban systems follows a non-linear path, with critical thresholds at which small local shocks can cause widespread systemic effects. This finding underscores the importance of continuous monitoring of early distortion indicators and developing preventive strategies that can identify and address vulnerabilities before they reach critical thresholds. The non-linear nature of urban distortion propagation also suggests that traditional risk assessment methods may underestimate the potential for cascading failures in highly connected systems.

The General Urban Distortion Propagation Law provides a conceptual and analytical framework that can support systemic risk assessment, subject to empirical calibration and validation to assess systemic risks in urban networks and identify cities with "systemic importance" that may serve as gateways for shock propagation. This analysis can guide resilience enhancement efforts toward areas with the greatest impact on overall system stability, optimizing resource allocation in resilience planning. By identifying key nodes and connections within the urban network, planners can prioritize interventions that provide the greatest systemic benefits.

This research provides a framework for developing integrated resilience strategies that take into account the connectivity between cities. Rather than focusing solely on enhancing the resilience of individual cities, the findings emphasize the importance of diversifying functional links and reducing excessive dependence on specific cities. This network-based approach to resilience planning represents a significant shift from traditional urban planning paradigms that often treat cities as independent entities.

The study highlights the need for better coordination between different administrative levels in risk planning and crisis response. The interconnected nature of urban risks requires coordinated responses that transcend traditional administrative boundaries, suggesting new governance models that can address the complex, cross-jurisdictional nature of urban resilience challenges in an increasingly connected world.

The application of the model faces challenges related to the availability of comprehensive and accurate data on functional links between cities, structural vulnerabilities, and recovery rates. There is a need for further research to develop alternative indicators and innovative data collection methods, leveraging big data techniques to operationalize the model's theoretical constructs. These methodological advances could significantly enhance the practical applicability of the GUDPL framework.

Future research could expand the model to include how shocks propagate between different neighborhoods and sectors within a single city, following a multi-level systems approach. There is also a need for further empirical verification of the model through detailed case studies of actual shock events, which could help calibrate the model and improve the accuracy of its predictions. Additionally, future research could explore how

the law can be integrated with other models, such as climate change or economic models, to develop a more comprehensive understanding of the multiple risks facing contemporary cities.

From a policy perspective, the GUDPL framework has the potential to support integrated risk assessment and resilience planning by enabling policymakers to identify systemically critical cities, vulnerable transmission pathways, and temporal windows for intervention. By translating complex intercity dependencies into an analytically tractable structure, the model can inform prioritization of infrastructure investment, emergency coordination, and resilience-enhancement strategies at regional and national scales. Moreover, the modular design of GUDPL facilitates future interdisciplinary applications, allowing integration with climate impact models, economic forecasting tools, and data-driven urban analytics platforms. This positions the framework as a flexible bridge between theoretical urban systems modeling and applied decision-support environments.

In a world of increasing connectivity and exposure to diverse shocks, understanding the dynamics of risk propagation across urban systems becomes critically important. The General Urban Distortion Propagation Law provides a theoretical and methodological framework that can contribute to the development of more resilient and sustainable cities and regions, offering a new lens through which to view and address the complex challenges of urban vulnerability in the 21st century.

References

Allen PM (1997) Cities and regions as evolutionary, complex systems. *Geographical systems* 4: 103–130

Alrasheed H, Alballa N, Al-Turaiki I, Almutlaq F, Alabduljabbar R (2024) City transmission networks: Unraveling disease spread dynamics. *ISPRS International Journal of Geo-Information* 13. CrossRef

Arieli I, Babichenko Y, Peretz R, Young HP (2020) The speed of innovation diffusion in social networks. *Econometrica* 88: 569–594. CrossRef

Avni N, Brenner N, Miodownik D, Rosen G (2022) Limited urban citizenship: The case of community councils in East Jerusalem. *Urban Geography* 43: 546–566. CrossRef

Barabasi AL, Pósfai M (2016) *Network Science*. Cambridge University Press, Cambridge, UK

Batty M (2005) *Cities and Complexity: Understanding Cities with Cellular Automata, Agent-Based Models and Fractals*. MIT Press, Cambridge, MA

Batty M (2013) *The New Science of Cities*. The MIT Press, Cambridge, MA. CrossRef

Berry BJL (1964) Cities as systems within systems of cities. *Papers in Regional Science* 13: 147–163. CrossRef

Bettencourt LMA, Lobo J, Strumsky D, West GB (2010) Urban scaling and its deviations: Revealing the structure of wealth, innovation and crime across cities. *PLoS ONE* 5: 13541. CrossRef

Boeing G (2021) Street network models and indicators for every urban area in the world. *Geographical Analysis* 54: 519–535. CrossRef

Borgatti SP, Brass DJ (2019) Centrality: Concepts and measures. In: Brass DJ, Borgatti SP (eds), *Social Networks at Work*. Routledge, 9–22. CrossRef

Buldyrev T, Parshani R, Paul G, Eugene S, Havlin S (2010) Catastrophic cascade of failures in interdependent networks. *Nature* 464. CrossRef

Coaffee J, Lee P (2016) *Urban resilience: Planning for risk, crisis and uncertainty*. Palgrave, London/New York

Crucitti P, Latora V, Porta S (2006) Centrality measures in spatial networks of urban streets. *Physical review. E*. CrossRef

Cutter SL, Burton CG, Emrich CT (2010) Disaster resilience indicators for benchmarking baseline conditions. *Journal of homeland security and emergency management* 7. CrossRef

Dorogovtsev SN, Goltsev AV, Mendes JF (2008) Critical phenomena in complex networks. *Reviews of Modern Physics* 80: 1275–1335 10 1103 80 1275. CrossRef

Fan C, Jiang X, Mostafavi A (2020) A network percolation-based contagion model of flood propagation and recession in urban road networks. *Scientific Reports* 10: 13481. CrossRef

Fotheringham AS, O'Kelly ME (1989) *Spatial Interaction Models: Formulations and Applications*. Kluwer Academic

Haynes KE, Fotheringham AS (1984) *Gravity and Spatial Interaction Models*. Sage Publication, Beverly Hills, CA

Hsu C, Fan C, Mostafavi A (2021). Limitations of gravity models in predicting fine-scale spatial-temporal urban mobility networks. CrossRef

Huff DL (1963) A probabilistic analysis of shopping center trade areas. *Land Economics* 39: 81–90. CrossRef

Hägerstrand T (1967) *Innovation Diffusion as a Spatial Process. Postscript and translation by Allan Pred*. The University of Chicago Press, Chicago and London

Lenormand M, Bassolas A, Ramasco JJ (2016) Systematic comparison of trip distribution laws and models. *Journal of Transport Geography* 51: 158–169. CrossRef

Linkov I, Trump BD, Trump J, Pescaroli G, Hynes W, Mavrodieva A, Panda A (2022) Resilience stress testing for critical infrastructure. *International Journal of Disaster Risk Reduction* 82: 103323. CrossRef

Lv Y, Sarker MNI, Firdaus RR (2024) Disaster resilience in climate-vulnerable community context: conceptual analysis. *Ecological Indicators* 158: 111527. CrossRef

Markolf SA, Chester MV, Eisenberg DA, Iwaniec DM, Davidson CI, Zimmerman R, Chang H (2018) Interdependent infrastructure as linked social, ecological, and technological systems (SETSs) to address lock-in and enhance resilience. *Earth's Future* 6: 1638–1659. CrossRef

Masucci AP, Serras J, Johansson A, Batty M (2013) Gravity versus radiation models: On the importance of scale and heterogeneity in commuting flows. *Physical Review E—Statistical, Nonlinear, and Soft Matter Physics* 88: 022812. CrossRef

Meerow S, Newell JP, Stults M (2016) Defining urban resilience: A review. *Landscape and Urban Planning* 147: 38–49. CrossRef

Peiris MTOV (2024) Assessment of urban resilience to floods: A spatial planning framework for cities. *Sustainability* 16: 9117. CrossRef

Pred A (1977) *City systems in advanced economies: Past Growth, Present Processes, and Future Development Options*. Wiley, London

Rahimi F, Sadeghi-Niaraki A, Ghodousi M, Choi SM (2025) Spatial-temporal modeling of urban resilience and risk to earthquakes. *Scientific Reports* 15: 8321. CrossRef

Reilly WJ (1931) *The law of retail gravitation*. Knickerbocker Press

Scott AJ, Storper M (2015) The nature of cities: The scope and limits of urban theory. *International journal of urban and regional research* 39: 1–15. CrossRef

Sharifi A, Yamagata Y (2017) Towards an integrated approach to urban resilience assessment. *APN Science Bulletin* 7. CrossRef

Simini F, González MC, Maritan A, Barabási AL (2012) A universal model for mobility and migration patterns. *Nature* 484: 96–100. CrossRef

Tang Y, Piao J, Wang H, Rajib S, Li Y (2025) Predicting cascade failures in interdependent urban infrastructure networks. *arXiv preprint*: 2503.02890. CrossRef

Taylor MO (2022) Spatial interaction modeling. In: Rey SJ, Franklin RS (eds), *Handbook of Spatial Analysis in the Social Sciences*. Edward Elgar Publishing, Chapter 12, 208–222,

Tubadji A, Rudkin S (2025) Cultural gravity and redistribution of growth through migration: Cohesion lessons from spatial econometrics and topological data analysis. *Papers in Regional Science* 104: 100064. CrossRef

Valdez LD, Shekhtman L, Rocca CE, Zhang X, Buldyrev SV, Trunfio PA, Havlin S (2020) Cascading failures in complex networks. *Journal of Complex Networks* 8: 013. CrossRef

Wang H, Zhao P, Yan XY (2023) Quantifying the overall characteristics of urban mobility considering spatial information. *arXiv preprint*: 2308.00975. CrossRef

Wang J, Kong X, Xia F, Sun L (2019) Urban human mobility: Data-driven modeling and prediction. *ACM SIGKDD explorations newsletter* 21: 1–19. CrossRef

Wilson AG (1970) *Entropy in Urban and Regional Modelling*. Pion Limited, Addison-Wesley Publishing, Boston

Yang Y, Herrera C, Eagle N, González MC (2014) Limits of predictability in commuting flows in the absence of data for calibration. *Scientific reports* 4: 5662. CrossRef

Yuan X, Geng H, Li Z (2025) Threshold effects of the interaction between urban development and atmospheric pollution. *Atmosphere* 16: 201. CrossRef

Zenou Y, Hodler R, Raschky P, Amarasinghe A (2018) Spatial diffusion of economic shocks in networks. CEPR Discussion Papers, https://ideas.repec.org/p/cpr/ceprdp/-12854.html

Zhang Y, Yang Y, Wei S, Ma Z, Tian M, Sun M, Nie J (2022) Research on spatial structure and resilience of complex urban network: A case study of Jing-Jin-Ji urban agglomeration. *Frontiers in Environmental Science* 10: 999124. CrossRef

Appendices: Numerical Operationalization of GUDPL Components (Proof-of-Concept)

These appendices provide the full numerical operationalization of the GUDPL components used in the proof-of-concept simulation presented in Section 3.1. All values are synthetic but designed to reflect plausible urban conditions. The purpose is to ensure transparency, replicability, and interpretability of the simulation results.

A Urban Network and Shock Context

Cities: A (shock origin), B, C, D, E

A.1 Shock origin (shock source city)

A.1.1 Shock origin city: City A

City A is the primary source node where the blackout initiates (e.g., major generation failure, substation cascade, or national dispatch collapse). It has the highest initial collapse intensity $E_0(A)$, and its downstream impacts propagate to other cities via directed functional couplings Φ_{ij} and time delays τ_{ij}.

A.2 Shock type

A.2.1 Shock type: Cascading power outage / grid failure (cascading blackout)

The shock propagates through electricity exchange capacity, industrial electricity dependence, and operational interconnection. These dimensions jointly define the functional coupling Φ_{ij}.

A.2.2 Collapse sub-indicators used to build $E_0(j)$:

I_{j1} : load-shedding ratio (power supply loss).
I_{j2} : Disruption of electricity-dependent critical services.
I_{j3} : Degradation in grid operational efficiency/stability.
All indicators are normalized to [0, 1] and aggregated using weights $\omega^{(E)}$.

A.2.3 The rationale for selecting the cascading blackout scenario as an illustrative case for the GUDPL model

The cascading power outage represents an ideal case study to illustrate the capabilities of the GUDPL model, as it embodies the core features the model is designed to capture. First, these shocks exhibit clear asymmetry in propagation, with influence flowing more strongly from cities with high generation capacity to those dependent on imports. Second, time delays τ_{ij} play a critical role, reflecting the operational and physical lags required for the disturbance to spread through the network. Third, the coupling between nodes Φ_{ij} depends on multiple dimensions (such as electricity exchange capacity, industrial dependence, and operational interconnectivity), enabling the representation of complex, nonlinear shock dynamics. Thus, this scenario provides a realistic and robust framework for testing the multidimensional, delayed, and asymmetric propagation mechanism that characterizes the GUDPL model.

A.3 Time horizon

Time horizon : $T = 8$ discrete steps. We simulate up to the final time index $T = 8$, i.e., $t \in \{0, \ldots, 8\}$. The horizon $T = 8$ is sufficient to capture the full propagation – attenuation – recovery cycle in the illustrative network, without loss of generality.
Time unit : *hours* (can be interpreted as hourly steps for blackout dynamics).
Simulation interval : $t = 0, 1, \ldots, T$ with $T = 8$.

A.4 Baseline attenuation (network-wide decay)

Baseline (system-wide) attenuation function :

$$R_s(t) = e^{-\lambda_s t}$$

Chosen baseline attenuation rate : $\lambda_s = 0.04$

The value $\lambda_s = 0.04$ is selected for illustrative purposes, representing moderate system-wide stabilization dynamics commonly observed in national-scale blackout recovery scenarios.

Interpretation : This captures system-wide fading of shock intensity over time due to overall stabilization efforts, national-level interventions, and progressive restoration in the network.

A.5 City-level recovery (exponential):

$$R_j(\Delta t) = e^{-\lambda_j \Delta t}, \quad \Delta t \geq 0$$

A.6 Additional core attenuation setting (distance attenuation)

Because the model also includes distance-based attenuation, we state it explicitly: $k = 1.25$.

Interpretation: Shock influence decays sub linearly-to-moderately with effective distance; appropriate for a shock that is not purely local but still attenuates as functional barriers increase.

A.7 Important consistency note

Because the model correctly defined $E_{\min,j}$ as an irreducible residual, it must not exceed the initial collapse intensity in the same city. Therefore, we explicitly enforce $E_{\min,j} \leq E_0(j)$ implemented as $E_{\min,j} = \min\left(E^{\text{raw}}_{\min,j}, E_0(j)\right)$. This is especially relevant for cities with very small initial $E_0(j)$.

B Structural vulnerability V_j (city-level)

The vulnerability weights used in this appendix follow a theory-informed, scenario-specific approach appropriate for proof-of-concept modeling. These weights are not treated as fixed parameters and can be recalibrated in applied or empirical extensions of the GUDPL framework.

B.1 Vulnerability Sub-Indicators

We compute vulnerability from three normalized sub-indicators:

V_{j1} : Grid infrastructure fragility (higher = worse)
V_{j2} : Economic dependence on electricity-intensive sectors (higher = worse)
V_{j3} : Institutional/operational capacity weakness (higher = worse)

B.1.1 Weights: $w^{(V)} = (0.40, 0.35, 0.25)$, $\sum w^{(V)} = 1$

The weighting approach is grounded in urban resilience and critical infrastructure literature. This approach is appropriate at the model-development stage, where the objective is to establish a generalizable mathematical framework rather than perform empirical calibration. The selected weights reflect the relative causal importance of infrastructure, economic structure, and institutional capacity in shock propagation. In applied studies, these weights can be recalibrated using analytic hierarchy processes (AHP), expert elicitation, or data-driven techniques such as entropy or principal component analysis.

B.1.2 Scientific Basis for Selecting Vulnerability Weights $w^{(V)} = (0.40, 0.35, 0.25)$

1. Conceptual rationale (theoretical grounding)

The weights assigned to the vulnerability dimensions were determined based on established principles in urban resilience theory, critical infrastructure studies, and cascading failure literature, which consistently emphasize that structural and physical conditions form the primary channel through which shocks materialize and propagate, followed by economic exposure and then institutional response capacity.

Accordingly, the vulnerability index V_j was decomposed into three dimensions with descending structural precedence:

a. Infrastructure vulnerability
b. Economic structural dependence
c. Institutional and governance capacity

This ordering reflects the causal hierarchy of collapse mechanisms observed in complex urban systems.

2. Justification of each weight component

(a) Infrastructure vulnerability — weight 0.40

Scientific basis:

- Infrastructure represents the *physical substrate* of urban systems.

Table B.1: Vulnerability sub-indicators used to construct the structural vulnerability index V_j

City	V_{j1}	V_{j2}	V_{j3}
A	0.70	0.60	0.65
B	0.40	0.45	0.35
C	0.55	0.70	0.55
D	0.30	0.35	0.30
E	0.50	0.40	0.45

- Failures in power grids, transport networks, water systems, or communications often act as initial triggers and amplifiers of cascading shocks.
- Infrastructure damage is frequently non-linear and partially irreversible, making it the dominant vulnerability dimension.

Support from literature (conceptual):

- Critical infrastructure theory treats physical networks as first-order determinants of systemic collapse.
- Network-based failure models show that infrastructure nodes often have high betweenness and load, magnifying propagation effects.

Interpretation in GUDPL:

- A higher weight (0.40) reflects the fact that even strong institutions or diversified economies cannot function without minimally operational infrastructure.

(b) Economic structural vulnerability — weight 0.35

Scientific basis:

- Economic structure determines how strongly a city is exposed to functional disruptions, especially in crises such as blackouts, supply-chain failures, or financial shocks.
- Cities with high sectoral concentration or electricity-intensive industries experience faster and deeper distortion once infrastructure is disrupted.

Why slightly lower than infrastructure:

- Economic impacts are often mediated by infrastructure availability.
- Economic systems are typically more adaptive than physical systems in the short term (e.g., substitution, inventory buffering).

Interpretation in GUDPL:

- The weight 0.35 reflects a secondary but still major role, capturing how shocks translate from physical disruption into systemic urban distortion.

(c) Institutional / governance vulnerability — weight 0.25

Scientific basis:

- Institutional capacity governs response speed, coordination, and recovery, rather than the immediate physical onset of collapse.
- Governance failures tend to shape duration and recovery trajectories, not necessarily the initial shock magnitude.

Why lower than the other two:

- Strong institutions mitigate rather than prevent physical or economic collapse.
- Their effects are often time-delayed, aligning with recovery functions $R_j(t)$ rather than initial vulnerability.

Interpretation in GUDPL:

- Assigning 0.25 ensures institutional factors are explicitly included, but without overstating their influence at the moment of shock propagation.

3. Methodological classification of the weighting approach

Formally, the chosen weights fall under "Theory-informed normative weighting". This approach is widely accepted when a new model is introduced, empirical calibration is not yet available, or the objective is demonstration of model operability, not parameter estimation.

In the GUDPL framework, weights are not fixed constants, but are scenario-dependent parameters, explicitly designed to be recalibrated.

B.2 Aggregate Vulnerability Computation

$$V_j = \sum_{\rho=1}^{3} \alpha_\rho v_{j\rho}$$

$\alpha_\rho = (0.40, 0.35, 0.25)$, $\sum_{\rho=1}^{3} \alpha_\rho = 1$

- $V_A = 0.40(0.70) + 0.35(0.60) + 0.25(0.65) = 0.6525$
- $V_B = 0.40(0.40) + 0.35(0.45) + 0.25(0.35) = 0.405$
- $V_C = 0.40(0.55) + 0.35(0.70) + 0.25(0.55) = 0.6025$
- $V_D = 0.40(0.30) + 0.35(0.35) + 0.25(0.30) = 0.3175$
- $V_E = 0.40(0.50) + 0.35(0.40) + 0.25(0.45) = 0.4525$

Based on these values, City A can be considered the most vulnerable (0.6525), followed by City C (0.6025), while City D is the least vulnerable (0.3175). This pattern is consistent with the underlying data, as Cities A and C exhibit higher values across the vulnerability sub-indicators.

C Initial Collapse Intensity

C.1 Collapse Intensity Sub-Indicators

For the power outage context, collapse intensity at $t = 0$ is constructed from three normalized sub-indicators:

I_{j1} : Power supply loss ratio (share of load shed)
I_{j2} : Critical service disruption (hospitals/water/pumping)
I_{j3} : Grid efficiency degradation (frequency/voltage instability proxy)

C.1.1 Weights: $w^{(E)} = (0.45, 0.35, 0.20)$, $\sum w^{(E)} = 1$

Weights assigned to collapse severity components $w^{(E)} = (0.45, 0.35, 0.20)$ were determined using a theory-informed, scenario-specific approach. The highest weight was assigned to immediate functional loss, as it represents the primary trigger and strongest driver of cascading effects in power outage scenarios. Critical service disruption was assigned a slightly lower weight, reflecting its role in amplifying and prolonging urban impacts. System efficiency degradation received a lower weight, as it primarily affects stability and recovery rather than the initial propagation of the shock. These weights are illustrative and can be recalibrated in applied studies using expert-based or data-driven methods.

C.1.2 Scientific Basis for Selecting Collapse Severity Weights $w^{(E)} = (0.45, 0.35, 0.20)$

1. Conceptual distinction (key clarification)

It is essential to distinguish between two different concepts in the GUDPL framework:

- V_j represents the *structural susceptibility* of city j to collapse.
- E_j represents the *realized collapse severity* resulting from an actual shock.

Accordingly, the weights $w^{(E)}$ are not derived using the same logic as vulnerability weights $w^{(V)}$, but are instead based on a dynamic, operational rationale linked to the moment of shock occurrence and its propagation through the urban system.

2. Definition of collapse severity components

In the selected shock scenario (cascading power outage), the collapse severity index E_j is constructed from three sub-components:

- Immediate functional loss (e.g., power supply loss or load-shedding ratio)
- Critical service disruption (e.g., hospitals, water pumping, and emergency services)
- System efficiency degradation (e.g., grid instability, frequency or voltage disturbances)

These components represent successive stages of collapse, rather than dimensions of equal influence.

3. Justification for individual weights

(a) Immediate functional loss — weight 0.45

Scientific basis:

Immediate functional loss represents the primary shock trigger (first-order shock). It is the most influential factor in:

- initiating cascading failure processes,
- determining the speed of shock propagation across the network,
- generating time delays τ_{ij}.

In power outage scenarios, loss of electricity supply is the event that initiates urban distortion and determines whether other systems are affected.

Reason for highest weight (0.45):

- It is the most time-sensitive component,
- and exhibits the highest potential for generating cascading effects.

(b) Critical service disruption — weight 0.35

Scientific basis:

This component reflects the transition from a technical failure to a system-wide urban crisis. While it is often temporally dependent on functional loss, it substantially amplifies and prolongs the shock's impacts.

Reason for slightly lower weight:

- It is causally downstream from immediate functional loss,
- yet more consequential than efficiency degradation in terms of social and humanitarian impact.

(c) System efficiency degradation — weight 0.20

Scientific basis:

System efficiency degradation captures the gradual structural deterioration of system performance. It is typically less visible at the moment of shock but is crucial for understanding the persistence of disruption.

Reason for lowest weight:

- It does not determine initial shock propagation,
- but primarily affects long-term stability and recovery trajectories, which are more directly associated with recovery functions $R_j(t)$.

4. Causal hierarchy underlying the weighting scheme

The ordering $0.45 > 0.35 > 0.20$ reflects a clear causal and temporal sequence:

1. Shock occurrence → immediate functional loss
2. Functional loss → critical service disruption
3. Prolonged disruption → system efficiency degradation

This hierarchy is not arbitrary, but mirrors both the order of occurrence and the order of influence in urban shock dynamics.

5. Methodological classification

The weighting scheme for $w^{(E)}$ falls under "Theory-informed, scenario-specific weighting". This approach is appropriate when the shock type is explicitly defined, the model is at a developmental stage, or the objective is to demonstrate dynamic behavior rather than empirical calibration.

C.2 Collapse Sub-Indicators and Raw Shock Magnitude S_j

We assume the initial shock originates in city A (primary collapse), while other cities have smaller initial disturbances.

Non-origin cities are assigned small baseline disturbances at $t = 0$ to reflect minor local susceptibility in blackout conditions. The dominant exogenous shock source remains city A.

These baseline disturbances do not represent independent shock sources, but latent instabilities that become relevant only through propagated coupling.

Table C.1: Collapse sub-indicators at $t = 0$ used to construct the raw shock magnitude S_j

City	I_{j1}	I_{j2}	I_{j3}
A	0.95	0.85	0.80
B	0.25	0.20	0.15
C	0.40	0.35	0.30
D	0.15	0.10	0.10
E	0.20	0.15	0.12

$$S_j = \sum_{m=1}^{3} \omega_m^{(E)} I_{jm}$$

$\omega_m^{(E)} = (0.45\ ,\ 0.35,\ 0.20), \quad \sum_{m=1}^{3} \omega_m^{(E)} = 1$

- $S_A = 0.45(0.95) + 0.35(0.85) + 0.20(0.80) = 0.885$
- $S_B = 0.45(0.25) + 0.35(0.20) + 0.20(0.15) = 0.2125$
- $S_C = 0.45(0.40) + 0.35(0.35) + 0.20(0.30) = 0.3625$
- $S_D = 0.45(0.15) + 0.35(0.10) + 0.20(0.10) = 0.1225$
- $S_E = 0.45(0.20) + 0.35(0.15) + 0.20(0.12) = 0.1665$

In the simulation, the values Sj are used directly as the initial collapse intensities $E_0(j)$.

Based on these values, The S_j represent the raw, unadjusted magnitude of the initial shock event at $t = 0$. The results clearly establish City A (0.885) as the epicenter of the crisis, with a collapse severity an order of magnitude higher than any other city. The small, non-zero values in other cities (e.g., City C at 0.363) reflect minor, localized instabilities inherent in the network even before the main shockwave propagates.

C.3 Realized Initial Collapse Intensity $E_0(j)$

$$E_0(j) = V_j * S_j$$

- $E_0(A) = 0.6525 * 0.885 = 0.5775$
- $E_0(B) = 0.405 * 0.2125 = 0.0861$
- $E_0(C) = 0.6025 * 0.3625 = 0.2184$
- $E_0(D) = 0.3175 * 0.1225 = 0.0389$
- $E_0(E) = 0.4525 * 0.1665 = 0.0753$

Based on these values, The final $E_0(j)$ represent the realized initial collapse intensity, factoring in both the shock's magnitude (S_j) and the city's inherent vulnerability (V_j). Although City A (0.578) remains the primary source, the high vulnerability of City C amplifies its minor initial disturbance into a more significant realized collapse ($E_0(C) = 0.218$), making it a secondary source of instability. In contrast, the low vulnerability of City D dampens its initial disturbance to a negligible level ($E_0(D) = 0.039$).

D Irreducible Residual Collapse

To reflect irreversible structural damage (e.g., transformer burnout), we set a parsimonious rule:

$E_{\min,j} = \min(\rho E_0(j), 0.30V_j)$, $\rho \in [0.2, 0.6]$. The parameter ρ controls the maximum fraction of the initial collapse that remains irreducible. In the illustrative simulation we set $\rho = 0.4$. Sensitivity can also be explored over $\rho \in [0.2, 0.6]$.

- $E_{\min,A} = 0.1958$
- $E_{\min,B} = 0.0344$
- $E_{\min,C} = 0.0874$
- $E_{\min,D} = 0.0156$
- $E_{\min,E} = 0.0301$

Table E.1: Directed functional coupling values Φ_{ij} between cities

$j \to i$	$L^{(1)}$	$L^{(2)}$	$L^{(3)}$	Φ_{ij}
$A \to B$	0.85	0.60	0.70	0.50(0.85)+0.30(0.60)+0.20(0.70)=0.745
$A \to C$	0.60	0.50	0.55	0.560
$A \to D$	0.35	0.30	0.25	0.315
$A \to E$	0.30	0.40	0.20	0.310
$C \to B$	0.55	0.50	0.45	0.515
$C \to D$	0.45	0.35	0.40	0.410
$C \to E$	0.40	0.30	0.35	0.360
$B \to D$	0.50	0.25	0.40	0.405
$B \to E$	0.35	0.30	0.30	0.325

Based on these values, The $E_{\min,j}$ quantify the permanent, irreversible damage that persists even after recovery efforts. The highest residual impact is assigned to City A (0.196), reflecting severe, lasting damage at the shock's origin. Notably, the value for City C (0.087) is also significant, indicating that its high vulnerability translates into a greater degree of permanent structural harm compared to less vulnerable cities like City D (0.016).

E Functional Coupling Φ_{ij}

For a blackout, functional coupling between j and i is built from three link types (normalized):

$L_{ij}^{(1)}$: Electricity exchange capacity (MW transfer potential, normalized)
$L_{ij}^{(2)}$: Industrial dependence of i on supply from j (normalized)
$L_{ij}^{(3)}$: Operational interconnection (shared substations/lines, normalized)

E.1 Weights

$\omega = (0.50, 0.30, 0.20)$, $\sum \omega = 1$

$$\Phi_{ij} = \sum_{r=1}^{3} \omega_r L_{ij}^{(r)}, \qquad \sum_{r=1}^{3} \omega_r = 1$$

In this proof-of-concept run, $\Phi_{j\to i}$ is treated as time-invariant for simplicity.

Note that $\Phi_{ij} \neq \Phi_{ji}$ in general, reflecting directional dependence and asymmetric intercity interactions.

E.2 Example Directed Linkage Values

In this appendix we use the directed notation $j \to i$ to indicate shock propagation from source city j to recipient city i. Accordingly, $j \to \Phi_i$, and $j \to \tau_i$ are defined on directed edges.

We list the edges used in the simulation (others assumed negligible/0 for compactness) in Table E.1.

All non-listed directed edges are set to 0 for compactness, yielding a sparse directed adjacency used in the proof-of-concept run.

Based on these values, The Φ_{ij} matrix quantifies the strength and direction of functional linkages, representing the pathways for shock propagation. The strongest coupling is from the shock origin to its immediate dependents, with $A \to B$ (0.745) being the most critical path. The matrix also reveals secondary propagation routes, such as $C \to B$ (0.515), indicating that City B is susceptible to shocks from multiple upstream sources. The sparse, directed nature of these values creates an asymmetric and realistic propagation network.

Table F.1: Effective distance components and aggregated effective distance d_{ij}

$j \to i$	$X_{ij}^{(1)}$	$X_{ij}^{(2)}$	$X_{ij}^{(3)}$	d_{ij}
$A \to B$	0.30	0.25	0.20	0.2575
$A \to C$	0.55	0.40	0.35	0.4475
$A \to D$	0.75	0.60	0.55	0.6475
$A \to E$	0.70	0.55	0.50	0.5975
$C \to B$	0.35	0.30	0.25	0.3075
$C \to D$	0.60	0.50	0.40	0.5150
$C \to E$	0.55	0.45	0.35	0.4650
$B \to D$	0.50	0.40	0.35	0.4275
$B \to E$	0.45	0.38	0.32	0.393

Note: To prevent unrealistic numerical amplification when some effective distances d_{ij} are very small (close to zero), a stability safeguard may be applied in general applications: $d_{ij}^{*} = \max(d_{ij}, \delta)$, with $\delta = 0.05$. In the present illustrative simulation, all $d_{ij} > \delta$. Therefore, results are unaffected.

F Effective Distance and Distance Attenuation

Effective distance is constructed from three normalized barrier dimensions (higher = harder for impact to travel):

- $X_{ij}^{(1)}$: restoration/response time barrier (normalized)
- $X_{ij}^{(2)}$: network constraint barrier (line redundancy weakness; barrier form)
- $X_{ij}^{(3)}$: institutional coordination barrier (normalized)

Weights: $\theta = (0.40, 0.35, 0.25)$, $\sum \theta = 1$

$$d_{ij} = \sum_{q=1}^{3} \theta_q X_{ij}^{(q)}$$

The distance attenuation exponent k is global for this illustrative run and set to $k = 1.25$. If "redundancy" is measured raw as Red_{ij} (higher = better), we normalize then invert:

$$\mathrm{Red}_{ij}^{\mathrm{norm}} = \frac{\mathrm{Red}_{ij} - \mathrm{Red}_{\min}}{\mathrm{Red}_{\max} - \mathrm{Red}_{\min}}, \quad X_{ij}^{(2)} = 1 - \mathrm{Red}_{ij}^{norm}$$

F.1 Barrier Dimensions

$$d_{ij} = \sum_{q=1}^{3} \theta_q X_{ij}^{(q)} = 0.40 X_{ij}^{(1)} + 0.35 X_{ij}^{(2)} + 0.25 X_{ij}^{(3)}$$

Note: Values of d_{ij}^{k} are computed numerically and rounded to three decimals for readability.

The d_{ij} values represent the functional "friction" or resistance to shock transmission, moving beyond simple geography. The path $A \to D$ (0.648) has the highest effective distance, suggesting significant barriers (e.g., institutional, network constraints) that will slow and weaken the shock's impact. Conversely, the path $A \to B$ (0.258) has the lowest distance, indicating a highly efficient channel for shock propagation.

F.2 Distance Attenuation d_{ij}^{k}

Now compute:

$$d_{ij}^{k} = (d_{ij})^{1.25}$$

The approximate values (sufficient for an illustrative appendix) are shown in Table F.2.

Table F.2: Distance-attenuated effective distances $(d_{ij})^k$ used in shock propagation

$j \to i$	d_{ij}	$(d_{ij})^{1.25}$
$A \to B$	0.2575	0.184
$A \to C$	0.4475	0.367
$A \to D$	0.6475	0.582
$A \to E$	0.5975	0.528
$C \to B$	0.3075	0.229
$C \to D$	0.5150	0.437
$C \to E$	0.4650	0.386
$B \to D$	0.4275	0.344
$B \to E$	0.393	0.311

Table G.1: Time delays τ_{ij} derived from effective distances

$j \to i$	d_{ij}	$\tau_{ij} = \left\lceil \frac{d_{ij}}{\nu} \right\rceil$
$A \to B$	0.2575	$\lceil 1.03 \rceil = 2$
$A \to C$	0.4475	$\lceil 1.79 \rceil = 2$
$A \to D$	0.6475	$\lceil 2.59 \rceil = 3$
$A \to E$	0.5975	$\lceil 2.39 \rceil = 3$
$C \to B$	0.3075	$\lceil 1.23 \rceil = 2$
$C \to D$	0.5150	$\lceil 2.06 \rceil = 3$
$C \to E$	0.4650	$\lceil 1.86 \rceil = 2$
$B \to D$	0.4275	$\lceil 1.71 \rceil = 2$
$B \to E$	0.393	$\lceil 1.57 \rceil = 2$

G Time Delay Specification τ_{ij}

We model delay as proportional to effective distance

$$\tau_{ij} = \left\lceil \frac{d_{ij}}{v} \right\rceil$$

with $v = 0.25$ (distance units per hour-step).

The ceiling operator ensures that propagation delays are not underestimated in discrete-time simulations. The results are shown in Table G.1.

The τ_{ij} values translate effective distances into discrete time steps (hours) required for the shock to travel. Impacts from the origin (A) will take 3 hours to reach the most functionally distant cities (D and E). In contrast, impacts arrive at the closest cities (B and C) in just 2 hours. This staggered timing is critical for understanding the cumulative, multi-wave nature of the distortion as it unfolds across the network.

H Recovery Functions and Network-Wide Decay

City-level recovery (exponential):

$$R_j(\Delta t) = e^{-\lambda_j \Delta t}, \qquad \Delta t \geq 0$$

Choose recovery rates (illustrative) from Table H.1.

Table H.1: City-level recovery rates λ_j and exponential recovery functions

j	λ_j	$R_j(\Delta t)$
A	0.10	(slowest recovery: source city with major damage)
		$R_A(\Delta t) = e^{-0.10\Delta t}$
B	0.14	$R_B(\Delta t) = e^{-0.14\Delta t}$
C	0.12	$R_C(\Delta t) = e^{-0.12\Delta t}$
D	0.18	$R_D(\Delta t) = e^{-0.18\Delta t}$
E	0.16	$R_E(\Delta t) = e^{-0.16\Delta t}$

The λ_j values represent the intrinsic recovery capacity of each city. The shock's origin, City A (0.10), is assigned the slowest recovery rate, reflecting major structural damage. In contrast, the most resilient city, City D (0.18), is given the fastest recovery rate. This inverse relationship between vulnerability and recovery speed is a core assumption, modeling the principle that more fragile systems struggle more to bounce back from disruptions.

Network-wide temporal decay:

$$R_s(t) = e^{-\lambda_s t}, \quad \lambda_s = 0.04$$

The separation between city-level recovery R_j and network-wide decay R_s allows the model to distinguish local repair capacity from systemic stabilization.

Note on the choice of t_0: In the main model (Eq. 4), the network-wide decay is written as $R_s(t - t_0)$, where t_0 denotes the network shock onset (or peak reference) time. In this simulation, the shock starts at $t = 0$. Therefore $t_0 = 0$ and $R_s(t - t_0) = R_s(t)$.

I Full dynamic GUDPL model (equation 4)

We use the deterministic illustrative setting $\varepsilon_i(t) = 0$ to make computations transparent.

$$D_i(t) = \left[\sum_{j=1}^{n} \frac{(E_{min,j} + (E_0(j) - E_{min,j})\ R_j\,(t - \tau_{ij}))\ \Phi_{ij}}{(d_{ij})^k} \right] R_s(t)$$

Arrival condition: if $t - \tau_{ij} < 0$, the term from $j \to i$ is set to 0 (impact has not arrived yet).

Note: In this proof-of-concept simulation, source collapse trajectories $E_j(t) = E_{\min,j} + (E_0(j) - E_{\min,j})R_j(t)$ are treated as exogenous inputs governed solely by city-level recovery dynamics. Endogenous feedback – where $E_j(t)$ depends on distortions received from other cities – is left for empirical calibration and future extensions of the model.

J Worked Simulation Examples

To demonstrate the operational application of the full GUDPL model (Equation 4), this section provides a detailed, step-by-step computation for two representative target cities: City B and City D. These cities were selected as illustrative cases (worked examples) to showcase how the model handles different scenarios of shock propagation: City B represents a case of rapid, high-intensity impact from a few sources, while City D illustrates a more complex case of delayed, cumulative impact from multiple upstream sources. The final simulation results for all affected cities (B, C, D, and E) are summarized in the concluding table of this appendix.

J.1 Pre-computed Constants and Gains

For convenience define the "propagation gain":

$$G_{ij} = \frac{\Phi_{ij}}{d_{ij}^k}$$

G_{ij} is introduced purely for computational convenience and does not alter the underlying structure of Equation (4). The computations for major edges are shown in Table J.1.

Define effective collapse in source city j at delayed time:

$$E_j^{\text{eff}}(\Delta t) = E_{\min,j} + (E_0(j) - E_{\min,j})\, e^{-\lambda_j \Delta t}$$

The G_{ij} values synthesize the relationship between functional coupling (Φ_{ij}) and distance-based attenuation (d_{ij}^k) into a single "propagation gain" multiplier for each path. The path $A \to B$ exhibits by far the highest gain (4.049), indicating that shocks originating from A are heavily amplified as they travel to B due to strong coupling and

Table J.1: Propagation gains G_{ij} for major directed paths

$j \to i$	Φ_{ij}	d_{ij}^k	$G_{ij} = \frac{\Phi_{ij}}{d_{ij}^k}$
$A \to B$	0.745	0.184	4.049
$A \to C$	0.560	0.367	1.526
$A \to D$	0.315	0.582	0.541
$A \to E$	0.310	0.528	0.587
$C \to B$	0.515	0.229	2.249
$C \to D$	0.410	0.437	0.938
$C \to E$	0.360	0.386	0.933
$B \to D$	0.405	0.344	1.177
$B \to E$	0.325	0.311	1.045

low effective distance. Conversely, the path $A \to D$ has a very low gain (0.541), meaning the impact is significantly dampened along this route. Table J.1 is crucial as it reveals the most critical and impactful propagation channels in the network.

J.2 Example: $D_B(t)$

Using the pre-computed propagation gains $G_{j\to i}$, delays $\tau_{j\to i}$, recovery rates λ_j, and residual terms $E_{\min,j}$, we compute $D_B(t)$ as follows. Contributions are set to zero when $t - \tau_{j\to B} < 0$.

City B receives propagated shock impacts mainly from two upstream cities: $j \in \{A, C\}$. Using the directed notation $j \to i$ (shock propagation from source j to recipient i), the distortion in city B at time t is computed as:

$$D_B(t) = \left[G_{A\to B} E_A^{\text{eff}}(t - \tau_{A\to B}) + G_{C\to B} E_C^{\text{eff}}(t - \tau_{C\to B}) \right] R_{s(t)}$$

Arrival condition: If $(t - \tau_{j\to B}) < 0$, the contribution from edge $j \to B$ is set to zero (impact has not yet arrived).
Delays: $\tau_{A\to B} = 2$, $\tau_{C\to B} = 2$.
Propagation gains: $G_{A\to B} = 4.049$, $G_{C\to B} = 2.249$.
Effective collapse in source city j at delayed time Δt is defined as:

$$E_j^{\text{eff}}(\Delta t) = E_{\min,j} + \left(E_0^{(j)} - E_{\min,j} \right) e^{-\lambda_j \Delta t}, \quad \Delta t \geq 0$$

Network-wide decay: $R_s(t) = e^{-\lambda_s t}$, with $\lambda_s = 0.04$.
Deterministic setting: $\varepsilon_B(t) = 0$.

At $t = 0$, 1 (No arrival yet):

$$D_B(0) = D_B(1) = 0$$

At $t = 2$ (arrival moment, $\Delta t = 0$):

$$E_A^{\text{eff}}(0) = E_0(A) = 0.5775$$
$$E_C^{\text{eff}}(0) = E_0(C) = 0.2184$$
$$R_s(2) = e^{(-0.08)} = 0.9231$$
$$D_B(2) = [4.049(0.5775) + 2.249(0.2184)](0.9231) = 2.612$$

At $t = 3$ ($\Delta t = 1$):

$$E_A^{\text{eff}}(1) = 0.1958 + (0.5775 - 0.1958)e^{(-0.10)} = 0.5412$$
$$E_C^{\text{eff}}(1) = 0.0874 + (0.2184 - 0.0874e^{(-0.12)} = 0.2036$$
$$R_s(3) = e^{(-0.12)} = 0.8869$$
$$D_B(3) = [4.049(0.5412) + 2.249(0.2036)](0.8869) = 2.349$$

At $t = 6$ ($\Delta t = 4$):

$$E_A^{\text{eff}}(4) = 0.1958 + 0.3817e^{(-0.40)} = 0.4516$$
$$E_C^{\text{eff}}(4) = 0.0874 + 0.1310e^{(-0.48)} = 0.1685$$
$$R_s(6) = e^{(-0.24)} = 0.7866$$
$$D_B(6) = [4.049(0.4516) + 2.249(0.1685)](0.7866) = 1.737$$

Interpretation: $D_B(t)$ peaks at the arrival time and then declines as recovery progresses, while remaining positive over the simulated horizon due to $E_{\min,j}$, while gradually attenuating under $R_s(t)$.

J.3 Example: $D_D(t)$

City D receives propagated shock impacts from three upstream cities:
$j \in \{A, C, B\}$
Accordingly, the distortion in city D at time t is computed as:

$$D_{D(t)} = \left[G_{A\to D}E_A^{\text{eff}}(t - \tau_{A\to D}) + G_{C\to D}E_C^{\text{eff}}(t - \tau_{C\to D}) + G_{B\to D}E_B^{\text{eff}}(t - \tau_{B\to D})\right] R_{s(t)}$$

At $t = 2$

Only the path $B \to D$ has arrived ($\tau_{B\to D} = 2$), while $A \to D$ and $C \to D$ have not yet arrived ($\tau_{A\to D} = \tau_{C\to D} = 3$).

$E_B^{\text{eff}}(0) = E_0(B) = 0.0861$, $Rs(2) = 0.9231$.

$$D_D(2) = [1.177 \times 0.0861] \times 0.9231 = 0.1013 \times 0.9231 = 0.094$$

At $t = 3$

Paths $A \to D$ and $C \to D$ arrive ($\Delta t = 0$), while Path $B \to D$ has $\Delta t = 1$.

$$E_A^{\text{eff}}(0) = 0.5775$$
$$E_C^{\text{eff}}(0) = 0.2184$$
$$E_B^{\text{eff}}(1) = 0.0344 + (0.0861 - 0.0344)e^{-0.14} = 0.080$$
$$Rs(3) = 0.8869$$
$$D_D(3) = [0.541 \times 0.5775 + 0.938 \times 0.2184 + 1.177 \times 0.080] \times 0.8869 = 0.542$$

At $t = 6$

$A \to D : \Delta t = 3$

$$E_A^{\text{eff}}(3) = 0.1958 + 0.3817e^{-0.3} = 0.4786$$
$$E_C^{\text{eff}}(3) = 0.0874 + 0.1310e^{-0.36} = 0.1788$$
$$E_B^{\text{eff}}(4) = 0.0344 + 0.0526e^{-0.56} = 0.0639$$
$$Rs(6) = 0.7866$$
$$D_D(6) = [0.541 \times 0.4786 + 0.938 \times 0.1788 + 1.177 \times 0.0639] \times 0.7866 = 0.395$$

Interpretation: City D experiences delayed but cumulative distortion driven by multiple upstream sources with heterogeneous arrival times. The distortion peaks shortly after the arrival of major contributors (A and C), then gradually declines due to recovery processes. However, $D_D(t)$ remains strictly positive because the irreducible residual term $E_{\min,j}$ prevents full disappearance of propagated effects, reflecting persistent structural damage within the network.

Table K.1: Final urban distortion trajectories $D_i(t)$ for all affected cities

Time (t)	$D_B(t)$ (Affected by A, C)	$D_C(t)$ (Affected by A)	$D_D(t)$ (Affected by A, C, B)	$D_E(t)$ (Affected by A, C, B)
0	0.000	0.000	0.000	0.000
1	0.000	0.000	0.000	0.000
2	**2.612** (Peak)	**0.814** (Peak)	0.094	0.271
3	2.349	0.732	**0.542** (Peak)	**0.543** (Peak)
4	2.118	0.661	0.486	0.488
5	1.916	0.598	0.437	0.439
6	1.737	0.542	0.395	0.397
7	1.578	0.493	0.358	0.360
8	1.438	0.449	0.325	0.328

K Final Simulation Results

The complete, corrected distortion trajectories $D_i(t)$ for all affected cities were computed iteratively for each time step from $t = 0$ to $t = 8$. The table below summarizes these final results, which form the numerical basis for the graphical analysis presented in the main body of the paper. This summary provides a comprehensive overview of the heterogeneous propagation dynamics across the urban network.

The final simulation results reveal clear and heterogeneous urban distortion dynamics shaped by the combined effects of functional coupling strength, effective distance, and propagation delays. City B exhibits the highest distortion levels across the entire time horizon, reaching its maximum at t=2 immediately upon shock arrival. This behavior reflects the exceptionally strong and short-distance coupling from the primary shock origin ($A \to B$), resulting in rapid and amplified impact transmission. In contrast, City C experiences a moderate and relatively simple response pattern, with a single early peak at $t = 2$ driven solely by its direct linkage to the origin city A, followed by a smooth monotonic decline governed by recovery dynamics.

Cities D and E display delayed but cumulative distortion profiles. Both cities register only minor impacts at t=2, corresponding to early arrivals from secondary upstream sources, and reach their respective peaks at $t = 3$ when the dominant contributions from cities A and C arrive simultaneously. This temporal superposition of multiple delayed sources generates a pronounced cumulative effect, clearly illustrating the model's ability to capture multi-source, time-staggered shock propagation. After their peak, distortion levels in both cities gradually decrease as recovery mechanisms take effect. However, distortions remain strictly positive over the simulated horizon due to the presence of irreducible residual components, which represent persistent structural damage within the network. Overall, the proof-of-concept results illustrate how GUDPL can represent immediate amplification, delayed accumulation, and recovery-driven attenuation under stylized assumptions.

L Optional Stochastic Term

If included, $\varepsilon_i(t) \sim N(0, \sigma^2)$ or a bounded noise scenario (e.g., $\pm 5\%$ of the deterministic $D_i(t)$). For transparency, all illustrative computations above assume $\varepsilon_i(t) = 0$.

M Implementation Pseudo-Algorithm

Input: City set $\mathcal{C}$, time horizon T, weights $w(V), w(E)$, parameters ω, θ, ρ, exponent k, delays τ_{ij}, recovery rates λ_j, system decay λ_s
Output: Distortion levels $D_i(t)$ for all cities i over time
`// Parameter domain`
$\rho \in [0.2, 0.6]$;
Step 1: Compute vulnerability
foreach *city* $j \in \mathcal{C}$ **do**
  Compute V_j from sub-indicators V_{jm};
end
Step 2: Compute shock intensity
foreach *city* $j \in \mathcal{C}$ **do**
  Compute S_j from indicators I_{jm};
  Compute $E_0(j) = V_j \cdot S_j$;
end
Step 3: Compute minimum shock level
foreach *city* $j \in \mathcal{C}$ **do**
  $E_{\min,j} = \min\left(\rho \cdot E_0(j),\ 0.30 \cdot V_j\right)$;
end
Step 4: Compute coupling strength
foreach *directed pair* (j, i) **do**
  Compute Φ_{ij} from network connectivity;
end
Step 5: Compute effective distance
foreach *directed pair* (j, i) **do**
  Compute d_{ij}^k;
end
Step 6: Temporal propagation
for $t = 0$ **to** T **do**
  Compute $R_s(t) = e^{-\lambda_s t}$;
  foreach *target city* $i \in \mathcal{C}$ **do**
    Initialize *total* $\leftarrow 0$;
    foreach *incoming city* j *with* $\Phi_{ij} > 0$ **do**
      if $t < \tau_{ij}$ **then**
        contribution $\leftarrow 0$;
      else
        $E_j^{\text{eff}}(t - \tau_{ij}) \leftarrow E_{\min,j} + (E_0(j) - E_{\min,j}) \cdot e^{-\lambda_j (t - \tau_{ij})}$;
        $\textit{contribution} \leftarrow \dfrac{E_j^{\text{eff}}(t - \tau_{ij}) \cdot \Phi_{ij}}{d_{ij}^k}$;
      end
      total $\leftarrow$ *total* + *contribution*;
    end
    $D_i(t) \leftarrow \textit{total} \cdot R_s(t)$;
    `// Optional noise term`
    $D_i(t) \leftarrow D_i(t) + \varepsilon_i(t)$;
  end
end

Algorithm M.1: Computational Implementation of the GUDPL Model